$2p3s3p$, $2p3p3p$, and $2p3s3s$ resonant Auger spectroscopy from NiO

M. Finazzi* and N. B. Brookes
European Synchrotron Radiation Facility, Boîte Postale 220, 38043 Grenoble Cedex, France

F. M. F. de Groot†
Solid State Physics Laboratory, University of Groningen, Nijenborg 4, 9747 AG Groningen, The Netherlands

(Received 2 April 1998)

We have investigated the behavior of the $2p3s3p$, $2p3p3p$, and $2p3s3s$ Auger lines of NiO, a model compound in the class of strongly correlated $3d$ systems, while varying the photon energy across the Ni L_3 and L_2 absorption edges. The experimental data are discussed in comparison with a theoretical model based on a charge-transfer multiplet approach. When the excitation energy is below the L_3 resonance, we observe the $2p3p3p$ and $2p3s3p$ peaks at a constant binding energy. This behavior is typical of nonradiative resonant Raman scattering. If the photon energy is increased further, the $2p3p3p$ and $2p3s3p$ lines rapidly transform into constant kinetic energy features, showing a normal Auger behavior. The transition from Raman- to Auger-like behavior takes place for photon energies lower than the ones corresponding to excitations of the photoelectron into ligand-hole states. This might indicate the participation of inelastic processes in the recombination of the core hole involving energies much smaller than the NiO gap, or the possible presence of nonlocal effects. On the high photon energy side of the L_3 edge, the constant kinetic energy of the $2p3p3p$ and $2p3s3p$ peaks is systematically larger than the one observed for an excitation well above the $L_{2,3}$ edges. We attribute this behavior to the intervention of an intermediate state of $2p^53d^{10}$ character, which has very little weight but is strongly enhanced at resonance. [S0163-1829(99)06215-3]

INTRODUCTION

With the availability of tuneable photon energy sources offered by synchrotron radiation facilities, resonant spectroscopy has become a powerful technique to study the electronic properties of condensed matter. For instance, the presence of a core hole in the intermediate state allows the study of the valence-band electronic structure, taking advantage of the site and symmetry selectivity typical of core spectroscopies. A recent development of this technique consists of exciting a core-hole with a well-defined moment with circularly polarized light, to be used as a probe to investigate the magnetic properties of the system under investigation.[1–3] For all these reasons, a better understanding of the core-hole recombination processes (Auger, x-ray emission) for resonance spectroscopies has become a very crucial topic.

It is well known that, for an excitation near an absorption threshold, the two-step model of the Auger or x-ray emission process often fails. The creation of a core hole and its radiative or nonradiative decay can no longer be considered as distinct independent processes, but they have to be viewed in a one-step model.[4] In this case, often called the resonant Raman regime, the energy position of the outgoing electron (Auger) or photon (x-ray emission) features follows the incoming photon energy, in contrast to the off-resonance excitation case, where the Auger (x-ray emission) lines appear at constant kinetic (photon) energy. The transition between Raman- and Auger-like behaviors depends on the possibility of the electron excited in the intermediate state losing energy or delocalizing faster than the lifetime of the initial core hole.[5] If this is the case, the electron in the intermediate state does not participate to the recombination of the core hole, carrying away the energy of the absorbed photon. In this way the electrons (photons) produced by the recombination of the core hole are detected at constant kinetic (photon) energy.

Recently, resonant Auger (RAES) and resonant x-ray emission (RXES) spectroscopies have also become important techniques to study the electronic properties of condensed matter. In solid state physics they have been widely employed in the investigation of core-excited states and of decay processes. For instance, Drube and co-workers reported the influence of the valence-band density of states in the $L_3M_{4,5}M_{4,5}$ resonant Auger of silver,[6] while Weinelt *et al.* investigated the interference effects in the Auger- and Raman-like regimes of the resonant valence-band photoemission of Ni metal.[7] Resonant Auger and x-ray scattering have also been performed at the Ca $L_{2,3}$ absorption edges of the highly ionic system CaF_2.[8–10] $L_{2,3}$-edge resonant x-ray scattering studies in MnO (Ref. 11) and NiO (Ref. 12) have recently been published, showing relaxation of the intermediate state, due to d-d and electron-hole pair excitation.

Here we present a study of the $2p3s3p$ ($L_{2,3}M_1M_{2,3}$), $2p3p3p$ ($L_{2,3}M_{2,3}M_{2,3}$), and $2p3s3s$ ($L_{2,3}M_1M_1$) Auger lines at resonance with the Ni L_2 ($\mathrm{Ni}\,2p_{1/2}\rightarrow\mathrm{Ni}\,3d$) and Ni L_3 ($\mathrm{Ni}\,2p_{3/2}\rightarrow\mathrm{Ni}\,3d$) absorption edges in NiO. We have chosen to study these Auger lines since their final states are characterized by two core holes, implying that they cannot be reached by any direct photoemission channel. This reduces the complexity of the problem as interference effects, such as those giving Fano line shapes, are not present. The experimental data are compared with the results of calculations including crystal-field effects and charge transfer.

NiO has long been considered as a prototype highly correlated compound since the observation that single-particle band calculations predict it to be metallic in contrast to the insulating nature of this system, characterized by a band gap of about 4 eV.[13,14] The nature of the gap (either Mott-Hubbard or charge transfer) has been at the center of the scientific debate for a long time.[15,16] The picture of NiO as a strongly correlated charge-transfer insulator was recently

TABLE I. Parameters defining the relative positions of the different configurations involved in the resonant (Raman) and nonresonant Auger $2p3p3p$ electron emissions. See text for the definition of $\Delta = 3.5$ eV, $U = 7$ eV, $Q_{2p} = 8.5$ eV, and $Q_{3p} = 8.25$ eV. The emitted free electrons are indicated as ε_P, ε_A, and ε_R, standing for photoemission electron, an Auger electron, and a Raman electron, respectively.

Ground state	$3d^8$	$3d^9\underline{L}$	$3d^{10}\underline{LL}'$
Weight	0.811	0.184	0.005
Relative energy (eV)	0	$\Delta = 3.5$	$2\Delta + U = 14$
Intermediate state—XAS	$2p^5 3d^9$	$2p^5 3d^{10}\underline{L}$	
Relative energy (eV)	$\Delta - Q_{2p} = -5$	$2\Delta + U - 2Q_{2p} = -3$	
Final state—Raman	$3p^4 3d^9 \varepsilon_R$	$3p^4 3d^{10}\underline{L}\varepsilon_R$	
Relative energy (eV)	$\Delta - 2Q_{3p} = -13$	$2\Delta + U - 4Q_{3p} = -19$	
Intermediate state—PES	$2p^5 3d^8 \varepsilon_P$	$2p^5 3d^9\underline{L}\varepsilon_P$	$2p^5 3d^{10}\underline{LL}'\varepsilon_P$
Relative energy (eV)	0	$\Delta - Q_{2p} = -5$	$2\Delta + U - 2Q_{2p} = -3$
Final state—Auger	$3p^4 3d^8 \varepsilon_P \varepsilon_A$	$3p^4 3d^9\underline{L}\varepsilon_P \varepsilon_A$	$3p^4 3d^{10}\underline{LL}'\varepsilon_P \varepsilon_A$
Relative energy (eV)	0	$\Delta - 2Q_{3p} = -13$	$2\Delta + U - 4Q_{3p} = -19$

confirmed by valence-band resonant photoelectron spectroscopy at the Ni $2p$ threshold.[17,18]

EXPERIMENT

The experiments were performed on the dragon beam line ID 12B at the European Synchrotron Radiation Facility,[19] using the circularly polarized light emitted by the helical undulator Helios I.[20] The slits of the monochromator were chosen to have a high counting rate in the electron analyzer. The photon-energy resolution was set to ~0.3 eV across the Ni L_2 and Ni L_3 edges, and to ~0.5 eV in the low-intensity regions of the absorption spectrum such as the pre-edge and between the L_2 and L_3. A clean (100) sample surface was obtained by cleaving *in situ* a NiO single crystal. The base pressure of the chamber was $<5\times10^{-10}$ mbar. The absence of carbon on the sample surface was monitored by measuring the C $1s$ core photoemission line. No detectable presence of carbon contamination was observed between two successive cleaves.

The energy distribution of the electrons excited in the vacuum by the x-ray beam was measured at normal emission using a commercial hemispherical analyser (PHI Model 3057, mean diameter 279.4 mm) with multichannel detection. The bandwidth of the analyzer was set to 0.25 eV, while its acceptance angle was $\pm 20°$. The direction of propagation of the photons defined an angle equal to $60°$ with the sample normal, while the (010) crystallographic axis of the sample was parallel to the plane containing the photon wave vector and the sample normal. In order to check and to correct possible shifts of the energy scale due to sample charging and/or drifts of the monochromator, the positions of the O $1s$ core photoemission line and of the valence-band maximum were measured for each spectrum.

THEORY

All the RAES spectra have been calculated with a Kramers-Heisenberg-type formula[4] using the charge-transfer-multiplet (CTM) model.[21,22] We find that the charge-transfer interaction has to be taken into account to obtain a good agreement between experimental and theoretical RAES, at variance with NiO RXES, where the experimental data can be well described by a model that does not include ligand-hole configurations in the basis dataset.[12] The necessity of including charge transfer will be even more apparent below, in the discussion about the photon-energy dependence of the binding-energy position of the RAES peaks.

The ground state of NiO is described as a linear combination of $3d^8$, $3d^9\underline{L}$ and $3d^{10}\underline{LL}'$ states, where $3d^9\underline{L}$ stands for nine $3d$ electrons and a hole in the oxygen valence band. The charge-transfer energy Δ, defined as the energy difference between $3d^8$ and $3d^9\underline{L}$, is 3.5 eV, while the correlation energy U is 7 eV.[22] Table I gives all the energy positions in the ground state, in the intermediate state with the $2p$ core hole, and in the final states with two core-holes in the $3s$ and/or $3p$ shells. The $2p$ core-hole potential Q_{2p} is assumed to be 8.5 eV, while the $3s$ and $3p$ core-hole potentials (Q_{3s} and Q_{3p}, respectively) are assumed to be 8.25 eV. Table I also contains the final states in case of off-resonance $3p3p$ Auger, which will be discussed below. Table I concerns only the effects of charge transfer, giving the relative energy positions of the various configurations. Important additional features are the atomic multiplet effects, also including the exchange interactions between the holes in the $3s$, $3p$, and $3d$ shells. The lifetime broadening of the intermediate states is assumed to be 0.2 eV in all cases, but we find that the shape of the theoretical RAES spectra is not very sensitive to significant variations of this parameter.

Table II describes in a systematic way all the multiplet parameters used for the ground and intermediate states. The parameters involved in the $2p3s3s$, $2p3p3p$, and $2p3s3p$ resonant Auger final states are also given. The atomic effects, i.e., the Slater integrals and the spin-orbit interactions, are calculated with an *ab initio* atomic program.[21] An ionic crystal field is added for all configurations. In the ground state, the $3d^8$ configuration is coupled to the $3d^9\underline{L}$ configuration with an e_g hopping (V_{e_g}) of 2.2 eV. The $3d^8$ configuration is affected by the spin-orbit interaction, by the Slater integrals, and by the ionic crystal field; $3d^9$ is influenced only by spin orbit and crystal field. Note that it is not neces-

TABLE II. Parameters used in the charge-transfer multiplet calculation of $2p3s3s$, $2p3s3p$, and $2p3p3p$ resonant Auger electron emission. The energy Δ_f, the spin-orbit couplings, the Slater integrals and the crystal field are given for each configuration, as well as the Auger matrix elements describing the decay and the hopping coupling the final states. The configurations are coupled by the hopping terms $V(e_g)$ and $V(t_{2g})$. Indicated is the value of $V(e_g)$. The t_{2g} hopping $V(t_{2g})$ is half this value. D_A is the dipole transition strength, and C_A the Auger matrix element. For the $3s3s$ final state, only the matrix element $\langle 2p\varepsilon|R^1|3s3s\rangle$ is present. All configurational parameters are given in eV units. See text for a detailed description.

Ground state	$3d^8$	$V_{e_g}=2.2$	$3d^9\underline{L}$	
	$\xi_d=0.08$		$\Delta=3.50$	
	$F^2_{dd}=9.79$		$\xi_d=0.08$	
	$F^4_{dd}=6.08$		$D_q=0.70$	
	$D_q=0.70$			
Intermediate state	$2p^53d^9$	$V_{e_g}=1.8$	$2p^53d^{10}\underline{L}$	D_A
	$\xi_p=11.51$		$\Delta_x=2.0$	[1.837]
	$\xi_d=0.09$		$\xi_p=11.51$	
	$F^2_{pd}=6.18$			
	$G^1_{pd}=4.63$			
	$G^3_{pd}=2.63$			
	$D_q=0.70$			
$3s3s$ final state	$3s^03d^9\varepsilon$	$V_{e_g}=1.8$	$3s^03d^{10}\underline{L}\varepsilon$	C_A
	$\xi_d=0.09$		$\Delta_f=-6.0$	$[R^1=0.19]\varepsilon_p$
	$D_q=0.70$			
$3p3p$ final state	$3p^43d^9\varepsilon$	$V_{e_g}=1.8$	$3p^43d^{10}\underline{L}\varepsilon$	C_A
	$\xi_p=1.41$		$\Delta_f=-6.0$	$[R^0=0.26]\varepsilon_p$
	$\xi_d=0.09$		$\xi_p=1.38$	$[R^2=0.18]\varepsilon_p$
	$F^2_{pp}=12.91$		$F^2_{pp}=12.73$	$[R^2=0.27]\varepsilon_f$
	$F^2_{pd}=14.37$			
	$G^1_{pd}=14.20$			
	$G^3_{pd}=8.66$			
	$D_q=0.70$			
$3s3p$ final state	$3s^13p^53d^9\varepsilon$	$V_{e_g}=1.8$	$3s^13p^53d^{10}\underline{L}\varepsilon$	C_A
	$\xi_p=1.40$		$\Delta_f=-6.0$	$[R^1=0.19]\varepsilon_s$
	$\xi_d=0.09$			$[R^0_E=0.23]\varepsilon_s$
	$F^2_{pd}=11.51$			$[R^1=-0.01]\varepsilon_d$
	$G^1_{pd}=14.22$			$[R^2_E=0.005]\varepsilon_d$
	$G^3_{pd}=8.67$			
	$G^1_{sp}=17.38$			
	$G^2_{sd}=10.86$			
	$D_q=0.70$			

sary to include $3d^{10}\underline{LL'}$ explicitly, as this configuration cannot reach an intermediate state. The dipole transition D_A projects the $3d^8$ configuration onto the $2p^53d^9$ configuration. In the intermediate state the spin-orbit interaction of the $2p$ core hole and its coupling to the $3d$ states due to the Slater integrals have to be included in the model. As there are nine $3d$ electrons, the d-d Slater integrals vanish. The $2p^53d^{10}\underline{L}$ state consists of a single peak at a relative energy (with respect to the $2p^53d^9$ configuration) of 2.0 eV (equal to $\Delta+U\text{-}Q_{2p}$), split only by the $2p$ spin-orbit coupling. The hopping in the intermediate and final states is assumed to decrease slightly due to the presence of the core hole(s). Evidence that this reduction actually takes place comes from recent resonant x-ray emission experiments.[11,23]

$2p3s3s$ resonant Auger lines

In the case of the $2p3s3s$ resonant Auger line, the final state is very simple. The $3s^03d^9$ state is split only by its $3d$ spin-orbit coupling and by the crystal field, both small. The

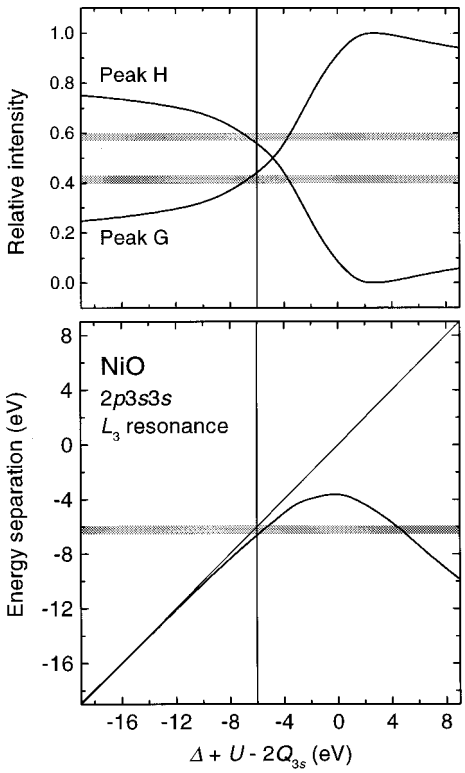

FIG. 1. Theoretical peak intensity (top) and energy separation (bottom) of the $3s^0 3d^9$ and $3s^0 3d^{10}\underline{L}$-derived lines in the $2p3s3s$ RAES as a function of $(\Delta+U-2Q_{3s})$. The incoming photon energy is assumed to be the one corresponding to the L_3 absorption edge maximum. The horizontal bars indicate the uncertainty of the experimental values. The vertical lines correspond to the value of $(\Delta+U-2Q_{3s})=-6.0$ eV that has been retained.

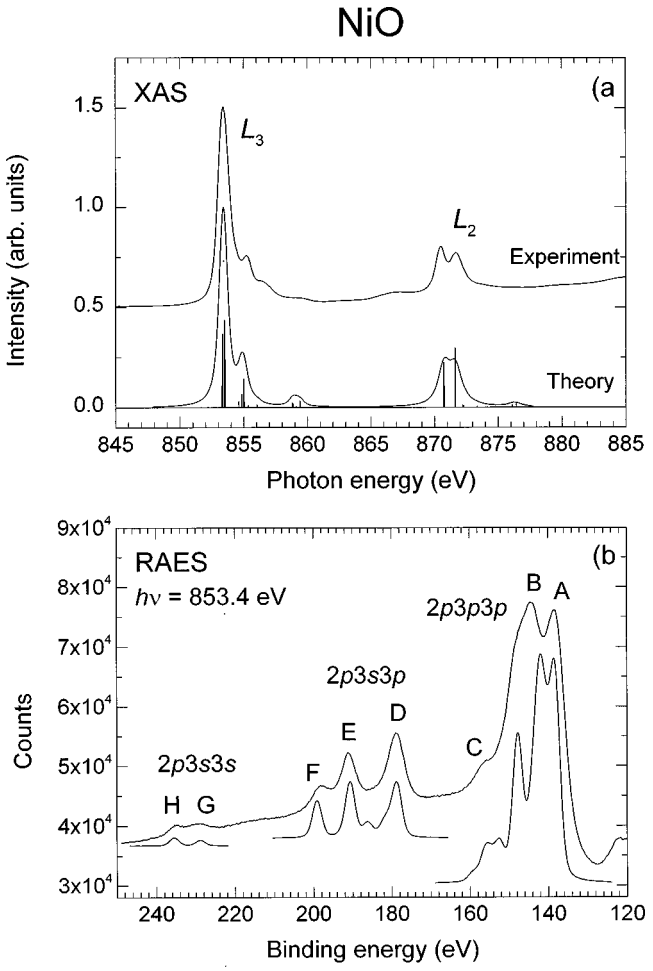

FIG. 2. Comparison between experimental data and atomic multiplet calculations (see text). (a) Ni $L_{2,3}$ absorption. (b) $2p3s3s$, $2p3s3p$, and $2p3p3p$ Auger lines at the Ni L_3 resonance ($h\nu$ = 853.4 eV). The energy scale of the theoretical absorption spectrum has been shifted to align the theoretical and experimental Ni L_3 maxima.

$3s^0 3d^{10}\underline{L}$ state is not split and is positioned at $(\Delta+U-2Q_{3s})=-6.0$ eV (see Table I). The final state thus essentially consists of two peaks, whose separation is directly related to the final-state energy difference between the two $3d^9$ and $3d^{10}\underline{L}$ configurations. Figure 1 shows the theoretical intensity and energy separation of the two $2p3s3s$ RAES main lines (corresponding to peaks *G* and *H* in Fig. 2) as a function of the final-state energy. Besides the two main lines, some minor side peaks are also present due to the spin-orbit splitting of the $3d$ band. In Fig. 1 these side peaks have been neglected.

In the limit of large negative (or positive) $\Delta+U-2Q_{3s}$ values, the two final states become pure $3d^9$ and $3d^{10}\underline{L}$. Their separation is roughly equal to $\Delta+U-2Q_{3s}$ and their intensity is proportional to the weight of the ionic configurations in the ground state (cf. Table I). In the case of smaller final-state energy differences, the effects of bonding and antibonding are larger. When the two lines cross over, the $3d^9$ and $3d^{10}\underline{L}$ configurations have almost equal weight in both the $2p3s3s$ peaks.

From Fig. 1 it can be concluded that the experimental peak separation and relative intensities of the $2p3s3s$ RAES spectrum allow for an accurate estimation of $\Delta+U-2Q_{3s}$. Since U and Q_{3s} are relatively well established, this also gives a good estimate of Δ.

$2p3s3p$ and $2p3p3p$ resonant Auger lines

In the case of the $2p3s3p$ resonant Auger line, the final state has $3s^1 3p^5 3d^9$ and $3s^1 3p^5 3d^{10}\underline{L}$ character (in hole notation $3s3p3d$ and $3s3p$, respectively). The ground and intermediate states are identical to the $2p3s3s$ case. For $2p3s3p$ RAES there are four different Auger matrix elements: $\langle 2p\varepsilon|R^1|3s3p\rangle$ and the exchange term $\langle 2p\varepsilon|R^0(E)|3s3p\rangle$ for an emitted electron of *s* symmetry, and $\langle 2p\varepsilon|R^1|3s3p\rangle$ and the exchange term $\langle 2p\varepsilon|R^2(E)|3s3p\rangle$ for an emitted electron of *d* symmetry. The effective cross section is almost 100 times larger for the emission of an *s* electron, and the emission of a *d* electron can be neglected. Table II contains all the final-state parameters for $2p3s3p$ and $2p3p3p$ RAES. In the case of $2p3p3p$ RAES, the intermediate state is coupled to an emitted *p* electron by R^0 and R^2 Auger matrix elements, and by a R^2 Auger matrix element to an emitted *f* electron. The cross section for the emission of a *p* electron is approximately ten times larger.

In $2p3s3p$ RAES, the accessible final states have the $3s3p$ hole configuration ($3s^1 3p^5 3d^{10}\underline{L}$) or the $3s3p3d$ hole

TABLE III. Symmetry, energy position, and multiplicity of the ionic $3s3p$, $3s3p3d$, $3p3p$, and $3p3p3d$ hole states given by the exchange interactions only. The plus (minus) sign of the symmetry states denotes parallel (antiparallel) core-hole spins. ^2P_i indicates an electron in the same hell.

State	Energy (eV)	Symmetry	Degeneracy
$3s3p$		$^2S\times{}^2P$	2×6
	−2.8672	$^3P+$	9
	8.6016	$^1P-$	3
$3s3p3d$		$^2S\times{}^2P\times{}^2D$	$2\times6\times10$
	−7.8036	$^4F+$	28
	−3.8450	$^2D+$	10
	−3.5411	$^4P+$	12
	−2.8646	$^4D+$	20
	2.3392	$^2F+$	14
	4.3678	$^2P+$	6
	9.5860	$^2F-$	14
	9.8501	$^2D-$	10
	10.8463	$^2P-$	6
$3p3p$		$^2P\times{}^2P_i$	$6\times5/2$
	−1.5275	$^3P+$	9
	1.5275	$^1D-$	5
	6.1098	$^1S-$	1
$3p3p3d$		$^2P\times{}^2P_i\times{}^2D$	$10\times6\times5/2$
	−5.8867	$^4F+$	28
	−4.5208	$^4D+$	20
	−4.2561	$^2F-$	14
	−3.8388	$^2P+$	6
	−0.2873	$^2G-$	18
	0.3469	$^4P+$	12
	1.6770	$^2D-$	10
	4.3085	$^2D-$	10
	5.6102	$^2S-$	2
	6.4744	$^2P-$	6
	8.8703	$^2F+$	14
	10.4766	$^2D+$	10

configuration. The only large interaction involved in the $3s3p$ state is the $3s3p$ exchange. There are two peaks separated by 10.47 eV, which is $\sim\frac{2}{3}$ times G^1_{sp}. In case of the $3s3p3d$ final state, large values are found for the $3s3p$, $3s3d$, and $3p3d$ exchange interactions. This results in a complex final state multiplet spread over some 18 eV. Table III reports all the energies and symmetries of the different multiplets involved. In Table III only the large exchange interactions (Slater integrals) have been included. It can be seen that the states lying at the lowest energies are the ones given by the Hund's rules with maximum spin and orbital moments. The states with the highest energies have antiparallel $3s$ and $3p$ spins. All the states are further affected by the crystal field (0.7 eV), the $3d$ spin-orbit coupling (less than 0.1 eV), and the $3p$ spin-orbit coupling (1.4 eV). Together they form the total multiplets of the $3s3p$ and $3s3p3d$ configurations, separated by the final-state energy difference of $\Delta+U-Q_{3s}-Q_{3p}=-6.0$ eV. The overall states in the spectra are then given by the bonding and antibonding combinations of the $3s3p3d$ states and the $3s3p$ states. The situation of the $2p3p3p$ RAES is similar, and all energies and symmetries are also given in Table III.

RESULTS AND DISCUSSION

As an example, Fig. 2 shows the comparison between the charge-transfer multiplet calculations and the experimental data for the Ni $2p$ absorption edges and the $2p3s3s$, $2p3p3p$, and $2p3s3p$ Auger lines at the Ni L_3 resonance ($h\nu=853.4$ eV). The final state binding energy (BE) is given by the photon energy minus the kinetic energy of the emitted electron, minus the work function of the analyzer (here assumed to be equal to 4.5 eV). The experimental absorption spectrum was obtained in the total-electron-yield (TEY) mode measuring the sample drain current. With the parameters given above, a reasonable agreement is obtained both for the x-ray-absorption spectroscopy (XAS) and for the RAES spectra at the same time. Concerning the $2p$ XAS spectrum of NiO, we would like to remark that the theoretical model contains only a single $3d^9\underline{L}$ configuration, and not a bandlike set of states. Inclusion of the actual band shape could improve the charge-transfer satellite region between $h\nu=858$ and 864 eV. In particular, a band structure with two maxima in the oxygen $2p$ valence band is able to reproduce the two satellite structures at $h\nu=859$ and 862 eV. The effects due to the details of the O $2p$ band on the RAES peaks are expected to be very small for photon energies far from the charge-transfer satellite region in the XAS spectrum. In particular, the multiplets contributing to the L_3 maximum depend very weakly on the shape of the valence band, and the resonant Auger across the L_3 main resonance are not affected considerably. For this reason, we chose not to complicate the theoretical model any further. Note also that the simulation of the L_2 edge is not as good as the L_3. To improve the overall agreement for both the L_3 and L_2 thresholds, one could use slightly different hopping values for the L_2 edge to include the effect of the continuum states.

The two-peaked $2p3s3s$ RAES spectrum is nicely reproduced. As described above, the peak separation is an important factor that settles the final state energy difference. In other words, in combination with the ground state and the x-ray-absorption spectrum, it settles the values of Δ, U, Q_{3s} and the hopping. The agreement is very good also between the experimental and theoretical $2p3s3p$ RAES spectra. The three main peaks are correctly reproduced, while the fourth peak just visible at a binding energy of 186 eV in the theoretical spectrum is smeared out by the lifetime broadening of the Auger lines.

The agreement between the theoretical and experimental $2p3p3p$ RAES is also reasonably good. The first peak is reproduced but the second structure at a binding energy of 144.5 eV (labeled B in Fig. 2), consisting in the experiment of a peak with a shoulder, in the theory appears as two peaks. This mismatch has to be probably ascribed to a poor estima-

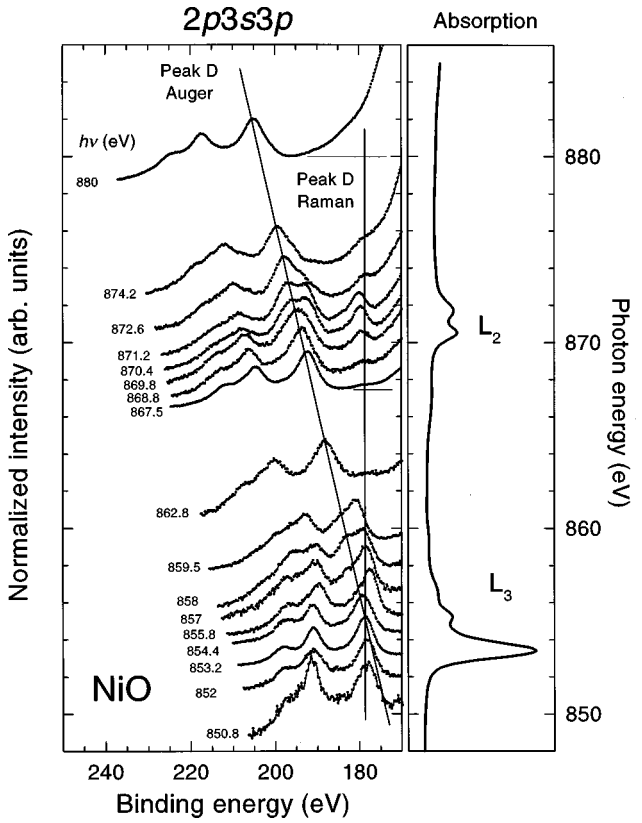

FIG. 3. Overview of a subset of the $2p3s3p$ spectra as a function of the photon energy. The spectra have been normalized to the intensity of peak D of Fig. 2(b).

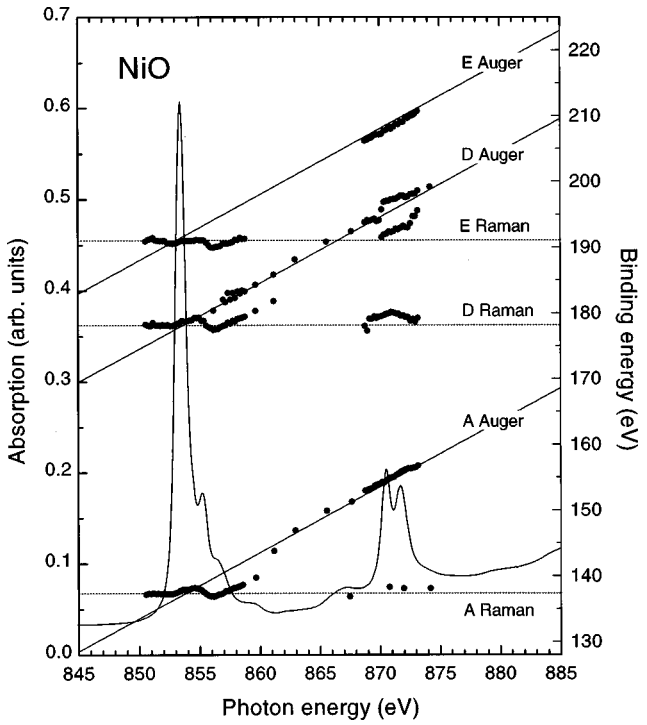

FIG. 4. Binding energy of peaks A ($2p3p3p$), D, and E ($2p3s3p$) as a function of the photon energy. The full straight lines correspond to constant kinetic energy points. They have been traced through the points corresponding to the positions of the peaks obtained at $h\nu=915$ eV.

tion of the value of the $3p3p$ and $3p3d$ exchange interactions used in the calculation. On the other hand, the structure labelled C at a binding energy of 157 eV is again nicely reproduced. It has been reported that the $2p3p3p$ channel interferes with the $2p3s3d$ channel.[22] At the L_3 resonance the $2p3p3p$ channel dominates and the effects of including this interference are minor. However, the effects on the $2p3s3d$ resonant photoemission spectrum are important.[22]

An overview of the $2p3s3p$ lines as function of the photon energy is shown in Fig. 3, where we plot a subset of the data. Also traced are the lines corresponding to the position of peak D [see Fig. 2(b)] in the case of Auger- or Raman-like behavior. Note that, for $856\leqslant h\nu<861$ eV and $870\leqslant h\nu<873$ eV, peak D appears to be split: it still shows features on the Auger line corresponding to off-resonance excitation, but a large part of its intensity lies at the right of this line, i.e., at lower binding energies. Note also that, even if the main D peak is observed around the Auger line, at the L_2 resonance some intensity is retrieved back in the Raman channel at a binding energy of 179.5 eV.

Figure 4 shows the final-state binding energy versus the photon energy dependence of the position of some of the peaks in the $2p3s3p$ and $2p3p3p$ lines. For clarity we show only the behavior of the sharp A, D, and E peaks [see Fig. 2(b)], since the position of the others is sometimes not very well defined. Focusing our attention to photon energies across the Ni L_3 edge only, we can distinguish three regions characterized by very different behaviors of the binding energy position of the RAES lines. They cover the photon energies (i) before the L_3 edge ($850\leqslant h\nu<852.5$ eV), (ii) across the L_3 absorption maximum ($852.5\leqslant h\nu<856$ eV), and (iii) between the L_3 and the L_2 edges ($856\leqslant h\nu<865$ eV), respectively.

In the first region, we observe the $2p3p3p$ and $2p3s3p$ peaks at constant binding energy. As illustrated above, this behavior is typical of the radiationless resonant Raman emission which is obtained when the photon energy is set below a threshold. Increasing the photon energy we enter the second region where, at $h\nu=853$ eV, the peaks seem to suddenly move to a $\sim$0.5-eV higher constant binding energy (also see Fig. 5). Above $h\nu=854$ eV, the peak position starts following an Auger line with constant kinetic energy. Because of the step at $h\nu=853$ eV, it is difficult to say exactly where the Auger behavior takes over from the Raman. However, note that the transition between these two regimes seems to occur already at $h\nu=854$ eV.

The transformation of the RAES peaks into constant kinetic energy features is obtained as a particular case of the one-step model when the photon energy is set at the onset of a band or a continuum of states.[4] This is the case, for instance, of Ni metal, where the Auger behavior is expected and observed as soon as the photon energy reaches the L_3 edge.[7] However, the case of the L_3 edge of NiO is completely different, due to the very localized nature of the $3d$ states. First, the Ni $4sp$ band can be immediately excluded from contributing to the transition to the constant kinetic-energy regime. In fact, the core-hole potential pulls the atomic-like Ni $3d$-derived states to much lower energies than the Ni $4sp$ band. The transitions to the Ni-$4sp$ continuum are visible as a step at $h\nu>866$ eV, i.e., at least 12 eV above the energy at which the Auger-like behavior sets in. Second,

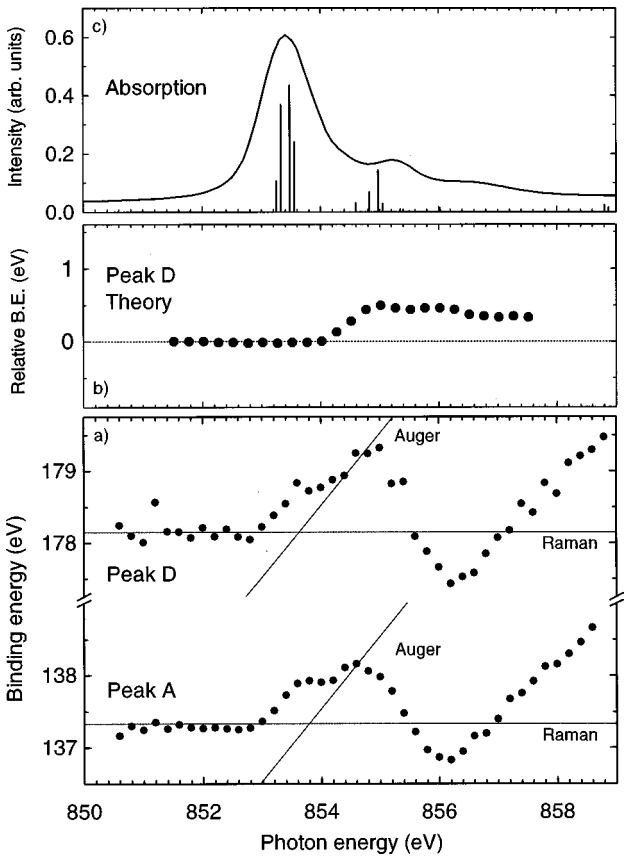

FIG. 5. Enlarged view of the experimental binding energy of the peaks A and D (a) compared to the theoretical position of peak D (b) as the incoming photon energy is scanned across the Ni L_3 absorption edge (c). The diagonal full straight lines in (a) have been traced as in Fig. 4. The energy scale in panel (b) has been determined as for Fig. 2(a). In panel (c), the full line is the experimental spectrum while the bars correspond to the theory.

at the L_3 edge, band states are involved only through hybridization between the Ni $3d$ orbitals and the O $2p$ ligands. However, the charge-transfer satellites contribute to the intermediate state only at photon energies above 856.5 eV (see Fig. 2), at least 2.5 eV above $h\nu = 854$ eV, where the transition from Raman to Auger electron emission is observed. Actually, the effect of the width of the O $2p$-derived band on the multiplets at the L_3 main resonance are minimal, as also demonstrated by the fact that, even if nonlocal screening is considered, the first ionization states will be atomic-like and only slightly affected by bandlike states.[24] Since at $h\nu = 854$ eV the intermediate state is still well localized around the absorbing atom, the RAES features should appear at constant binding energy unless relaxation channels are present.[25] These observations might indicate the participation of inelastic processes in the recombination of the core-hole involving energies much smaller than the NiO charge-transfer gap. Another possibility is that nonlocal effects are still important in the intermediate state reached at the main resonance of the L_3 absorption edge, and that they can contribute to its relaxation. It is difficult to determine the nature of the relaxation processes from our data. Just above the edge the system must find a mechanism to lose its energy, for example by exciting a phonon, a magnon, a transition between impurity states into the gap, etc. This important problem can best be studied if an x-ray energy resolution of 0.1 eV, or possibly better, is used. However, as we show below, the photon-energy dependence of the peak position around threshold is more complicated than a simple transition from Raman- to Auger-like behavior.

Note that in the RXES spectra of NiO a significant ($\sim$20%) Raman contribution is still visible for energies of the incoming electron as high as 5–6 eV above the Ni L_3 edge.[12] In contrast, we cannot identify any Raman-like feature in the RAES spectra for $h\nu > 854.5$ eV, mainly because the complicated structure of the RAES lines and the large core-hole lifetime broadening smear any weak feature into the dominant Auger peaks.

In the third region, between $h\nu = 854.5$ and 856 eV, the position of the peaks suddenly drops, and above 856 eV it seems to follow an Auger line again, at a different constant kinetic energy. A rather interesting observation is that this Auger line has no relation to any peak in the off-resonance Auger spectrum (see Fig. 4). Only for peak D do we still see a feature at the kinetic energy corresponding to the off-resonance case. At higher energies ($h\nu > 861$ eV) the peak position shifts back to the original Auger line, which is also the dominant peak across the L_2 resonance and off resonance. Note that, in the L_2 region, only peak D still appears to be split into two components: the first on the line corresponding to the off-resonant Auger and the second at higher kinetic energy. At least three mechanisms can be invoked to explain the behavior of the RAES at the L_3 resonance: experimental artifacts, multiplet effects, and ''hidden'' states.

Experimental artifacts

A potential experimental artifact, also discussed in Ref. 26, is related to insufficient resolution of the x-ray monochromator. Assume for example a square box-shaped resolution function with a 1-eV width, and also assume a single resonance with a lifetime broadening of 0.2 eV. Then, as long as the system presents an intermediate state whose resonance energy is within this 1 eV, it will resonate in the same anner scanning the photon energy. If the peak intensity is plotted as a function of the excitation energy, which is the average energy of the 1-eV region, a peak with constant kinetic energy is observed (i.e., Auger behavior). Excitation energies for which the peak position lies (significantly) below or above the resolution window will show the expected peak at a constant binding energy (i.e., Raman behavior). With a Gaussian-shaped resolution function this behavior is less strong, but still present. Thus, if the experimental resolution of the x-ray monochromator is ''poor,'' say larger than the lifetime broadening of the resonance(s), this results in an ''artificial'' constant kinetic-energy peak being found. In the present case, the resolution is 0.3 eV across the L_3 edge, and such effects should be limited. Note that the resolution of the detector has no influence at all.

Multiplet effects

In the case of CaF_2, it has been shown that for the resonant photoemission spectra[10,27] as well as the resonant x-ray Raman spectra,[28] multiplet and crystal-field effects can modify the peak positions of the resonant spectra. The basic idea of the resonance (as discussed in the Introduction) as-

sumes an effective transition (via a ''virtual'' intermediate state) from the ground state to a final state, resulting in a peak at the binding energy of this final state. In many cases the influences on the energy position of the peaks due to crystal-field effects (and approximately also of exchange) are similar in the intermediate and final states. Assume that one has a ground state G, two intermediate states I_1 and I_2, and two final states F_1 and F_2. The basic theory then expects two peaks at the constant binding energies related to F_1 and F_2. However, now assume that I_1 decays essentially to F_1, and I_2 essentially to F_2 (generally this happens only when the splitting in the intermediate and the final state is about the same); then a single peak is observed, resulting from the $I_1 \rightarrow F_1$ or $I_2 \rightarrow F_2$ transition. Its binding energy will be constant as long as the intermediate state has either mostly I_1 or mostly I_2 character, and will correspond to the one related to F_1 or F_2, respectively. If one shifts the excitation energy from I_1 to I_2, the final state will change from almost pure F_1 to almost pure F_2, shifting intensity over the spectral shape. More precisely, the peaks in the Auger spectrum will appear to move to higher binding energy as the photon energy is increased (if the intermediate state is not relaxed). The analysis of CaF_2 showed that this actually happens in the case of crystal-field-split states.[10,27,28]

In the present situation the exchange interactions of the $2p$ hole can be expected to be drastically different from those of the $3s$ and $3p$ holes. Only the crystal-field effect should be similar in the intermediate and final states. Therefore, one can set an upper limit of 0.7 eV to the constant kinetic-energy shift due to intensity transfer over multiplet-induced peaks. Figure 5 shows the binding energy of peaks A and D as the incoming photon energy crosses the Ni L_3 white line. The position of peak D predicted by the CTM model is also indicated. Note that, since the model is local, the calculation cannot describe the observed Raman to Auger transformation. The theoretical BE of peak D shows a 0.55-eV shift toward higher BE after the L_3 maximum, at $h\nu = 854.5$ eV, due to the transfer of spectral weight across different crystal-field-split multiplets. In the experimental data, the peak position presents a kink already at $h\nu = 853.2$ eV, i.e., before the Ni L_3 edge. The observation that the shift of the experimental position of the RAES peaks occurs at a photon energy much lower than expected by the theory seems to exclude transfer of spectral weight between different Raman lines. More probably, the step at $h\nu = 853.2$ eV could be due to changing from a Raman- to an Auger-like regime. The Auger-like behavior could be due either to the photon-energy resolution effects described above or to Auger recombination of relaxed lifetime broadened multiplets [note that the lowest-energy multiplet in the calculated absorption spectrum of Fig. 2(a) lies at $h\nu = 853.25$ eV]. We believe that the two phenomena are present at the same time, since the Auger-like behavior is observed for $853.2 \leqslant h\nu < 854.2$ eV, while experimental artifacts might be important only over a range limited to the energy resolution of the monochromator ($\sim$0.3 eV).

Multiplets effects are probably visible around $h\nu = 854$ eV, where the position of the peaks shows a second step. In this case, it is difficult to say if we assist to a transition between different Raman lines at constant BE (as expected by the one-step model) or between two distinct Auger-like lines (either due to photon-energy resolution artifacts or to relaxation of the intermediate state) at constant kinetic energy. In both cases, the transition will be induced by excitation into distinct relaxed (Auger behavior) or unrelaxed (Raman behavior) intermediate-state multiplets that selectively decay into different final states. Note that the photon energy position of this second step is very similar to the ones obtained from the CTM model, reinforcing the hypothesis of the presence of multiplet effects.

An interesting observation is that, while we find that the theoretical photon dependence of the binding energy of peaks D and E is basically the same, peak F does not show any theoretical shift. The reason is related to peak F having mostly charge-transfer character ($3d^{10}\underline{L}$). This fact could be used as a diagnostic to prove if multiplet effects are really responsible of the kink we observe at $h\nu = 854$ eV, or if different mechanisms have to be considered. Unfortunately, we cannot determine the kinetic energy of peak F with a high enough accuracy to say if it moves to higher values or stays constant.

''Hidden'' states

The mechanisms illustrated above cannot account for the constant kinetic energy peaks visible between $h\nu = 855.6$ and 861 eV. These Auger peaks are not visible off-resonance, where they can be considered to be ''hidden.'' To explain the nature of this peak, we go back to Table I, which indicates the energy positions of the states in XAS and Raman (top) and for photoemission spectroscopy (PES) and Auger (bottom). In XAS, about 80% of the total intensity goes into the $3d^9$ intermediate state configuration and about 20% into the $3d^{10}\underline{L}$ intermediate state configuration. In PES, $\sim$80% of the total intensity goes into the $3d^8$, configuration $\sim$20% into the $3d^9\underline{L}$ configuration and less than 1% into the $3d^{10}\underline{L}\underline{L}'$ configuration (note that the actual states are linear combinations of $3d^8$, $3d^9$, and $3d^{10}$ configurations, and that there is interference). Thus the $3d^{10}$ state is part of the PES intermediate state, but has no or little weight. This implies that the peak associated with its related Auger final state also has no intensity. It is actually this configuration that has the lowest binding energy in the final state due to the two $3p$ holes, and hence a relative energy position of $-4Q_{3p}$. Excitations to the charge-transfer satellite at about 5 eV above the edge reach intermediate states dominated by $2p^5 3d^{10}\underline{L}$. The relaxed intermediate state contains $2p^5 3d^{10}$ character, which can decay to the $3p^4 3d^{10}$ (or $3s^1 3p^5 3d^{10}$) final state. Since at resonance the intensity of the Auger lines follows the XAS dipole transition cross section, the intensity reaching this final state is much larger than off resonance (cf. Table I). Thus this state, which was hidden in the off-resonance Auger regime, becomes visible in the on-resonance Auger regime while exciting into the charge-transfer satellite. Actually, we already observe these peaks at photon energies as low as 856 eV, well below the position of the ligand-hole satellite centered at $h\nu = 859$ eV in the absorption spectrum. Moreover, the sudden drop of the BE position of the RAES peaks for $854.5 < h\nu < 856$ eV in Fig. 5 is already probably due to transfer of spectral weight to the ''hidden'' peaks. This is not incompatible with the interpretation we have given above, since in the intermediate-state

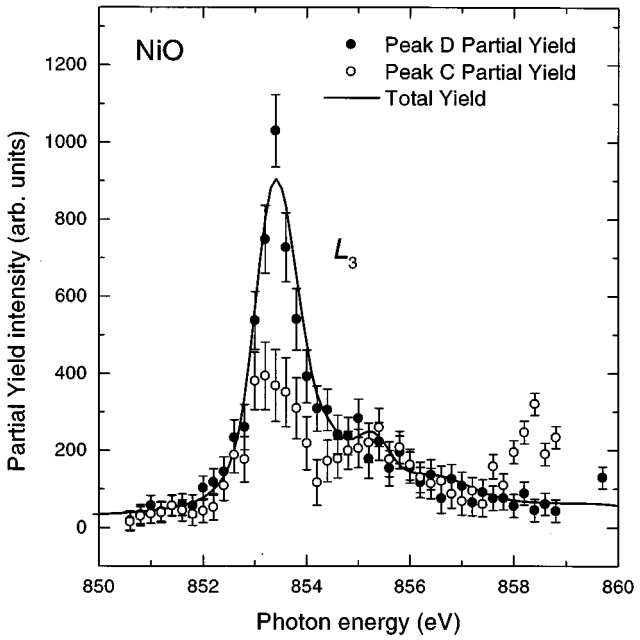

FIG. 6. Intensity of peaks *D* and *C* as a function of the photon energy compared to the TEY spectrum.

lifetime effects broaden the multiplets and hybridization mixes peaks of $2p^5 3d^9$ and $2p^5 3d^{10}\underline{L}$ character.

In this context, the off-resonant Auger spectrum results from the decay of a relaxed intermediate state of mostly $2p^5 3d^9$ symmetry. In principle, the Auger electrons emitted as a consequence of the core-hole recombination of these relaxed states should also be observable in the energy range where the ''hidden'' states become visible. For this reason, all the RAES peaks should be accompanied by lines at a kinetic energy corresponding to the off-resonance Auger spectrum, as we see for peak *D*. In practice, however, these components are only resolved in connection to peak *D*.

Partial yield

Figure 6 shows the partial yield intensity of peaks *D* and *C* of Fig. 2(b) as a function of the photon energy across the L_3 absorption edge [the dependence of peaks *B* and *E* of Fig. 2(b) is essentially the same as the one observed for peak *D*. Peak *F* shows a behavior more similar to peak *C*]. Note how the partial yield of peak *D* follows the total TEY absorption intensity, as expected for Auger transitions with a final state that cannot be reached by a direct dipole transition, thus excluding the possibility of interference with normal photoemission.[9] The fact that peak *C* does not resonate as much as peak *D* can be interpreted as a consequence of the predominant charge-transfer character of peak *C*. Actually, the constant final-state spectra calculated for peaks *F* and *D* show that, compared to the partial yield of peak *D*, the charge-transfer satellite *F* has a lower intensity when the photon energy corresponds to the L_3 maximum ($h\nu = 853.4$ eV), and a higher intensity on the TEY shoulder at $h\nu = 855.2$ eV. However, this effect is not as large as observed in Fig. 6. One reason for this could be too small a final-state hopping in the theoretical model.

Since in the energy range across the L_3 edge the position of peak *D* follows the photon energy, the partial yield spectrum is dominated by the $2p_{3/2}$ core-hole lifetime.[29] One-step models of the Auger process predict that at resonance the broadening of the Auger lines might be reduced.[4] The analysis of the full width at half maximum of peak *D* shows that if such an effect is present, it is smaller than the resolution of the electron energy analyzer (~0.25 eV).

L_2 resonance

At the L_2 edge, peaks *A* and *D* evolve into two structures (see Fig. 4). The first one is the Raman feature, visible across all the L_2 resonance at a constant binding energy corresponding to the pre-L_3 edge Raman peak. The second is the Auger peak related to the relaxed Auger of the L_3 edge, which appears at about the same kinetic energy as the off-resonance Auger. Note that the Auger peak associated to the $2p^5 3d^{10}$ intermediate state is still visible in the $2p3s3p$ L_2 RAES, but is weaker than at the L_3 edge.

In principle, one could expect additional peaks, such as an Auger structure related to the L_2 edge itself ($2p_{1/2}3p3p$ Auger). In fact, in Ni metal this L_2 Auger peak is visible.[7] Another possible decay channel could be the L_3 Raman channel, represented by the one-step recombination of the $2p_{3/2}$ core hole resulting after a $2p_{1/2} \rightarrow 2p_{3/2}$ Coster-Kronig transition. The absence of the L_3 Raman peak at the L_2 edge indicates that the Coster-Kronig decay produces a relaxed intermediate state. The presence of the L_2 Auger peak in Ni metal and its absence in NiO indicates that for NiO the Coster-Kronig decay dominates the production of a relaxed intermediate state in the presence of a $2p_{1/2}$ core hole. It is in fact somewhat surprising that this channel is seen for Ni metal.[7] As indicated above, the study of this core-hole dynamics can be greatly refined by using as high an x-ray energy resolution as possible.

CONCLUSIONS

We have studied the $2p3s3s$, $2p3p3p$, and $2p3s3p$ Auger lines at resonance with the Ni $L_{2,3}$ absorption edges in comparison with a charge-transfer multiplet model. When the photon energy is below the L_3 resonance, the $2p3p3p$ and $2p3s3p$ peaks appear at a constant binding energy, as expected for a nonradiative Raman process. The behavior of the RAES lines becomes much more complicated as the photon energy is scanned across the L_3 absorption maximum, where symmetry-dependent multiplet effects are probably present. If $h\nu$ is increased further, the $2p3p3p$ and $2p3s3p$ lines show a normal Auger behavior, with peaks at a constant kinetic energy. The transition between these two regimes occurs at photon energies lower than those corresponding to excitations of the photoelectron into ligand-hole states. This might indicate the participation of inelastic processes in the recombination of the core hole, involving energies much smaller than the NiO gap, or the presence of nonlocal effects. On the high-energy side of the L_3 edge, the constant kinetic energy of the $2p3p3p$ and $2p3s3p$ peaks is systematically larger than the one observed for an excitation well above the $L_{2,3}$ edges. This is due to the intervention of a relaxed intermediate state of $2p^5 3d^{10}$ character, which has very little weight but is strongly enhanced at resonance.

ACKNOWLEDGMENTS

F.dG. was funded by the Royal Netherlands Academy of Arts and Sciences (KNAW). We are grateful to P. L. Wincott and G. Thornton (Manchester University) for providing the NiO single crystal. We would also like to thank L. H. Tjeng and L. Braicovich for stimulating discussions, and Kenneth Larsson for his invaluable technical assistance.

*Present address: TASC-INFM, Elettra Synchrotron Light Source, Strada Statale 14 Km. 163.5, AREA Science Park, 34012 Basovizza, Trieste, Italy.

†Present address: Department of Inorganic Chemistry, Debeye Institute, University of Utrecht, Sorbonnelaan 16, 3584 CA Utrecht, The Netherlands.

[1] B. T. Thole, H. A. Dürr, and G. van der Laan, Phys. Rev. Lett. **74**, 2371 (1995).

[2] L. H. Tjeng, B. Sinkovic, N. B. Brookes, J. B. Goedkoop, R. Hesper, E. Pellegrin, F. M. F. de Groot, S. Altieri, S. L. Hulbert, E. Shekel, and G. A. Sawatzky, Phys. Rev. Lett. **78**, 1126 (1997).

[3] B. Sinkovic, L. H. Tjeng, N. B. Brookes, J. B. Goedkoop, R. Hesper, E. Pellegrin, F. M. F. de Groot, S. Altieri, S. L. Hulbert, E. Shekel, and G. A. Sawatzky, Phys. Rev. Lett. **79**, 3510 (1997).

[4] T. Åberg and B. Crasemann, in *Resonant Anomalous X-Ray Scattering*, edited by G. Materlik, C. J. Sparks, and K. Fischer (Elsevier, Amsterdam, 1994), p. 431.

[5] O. Karis, A. Nilsson, M. Weinelt, T. Wiell, C. Puglia, N. Wassdahl, N. Mårtensson, M. Samant, and J. Stöhr, Phys. Rev. Lett. **76**, 1380 (1996).

[6] W. Drube, A. Lessmann, and G. Materlik, in *Resonant Anomalous X-Ray Scattering* (Ref. 4), p. 473; W. Drube, R. Treusch, and G. Materlik, Phys. Rev. Lett. **74**, 42 (1995).

[7] M. Weinelt, A. Nilsson, M. Magnuson, T. Wiell, N. Wassdahl, O. Karis, A. Föhlisch, N. Mårtensson, J. Stöhr, and M. Samant, Phys. Rev. Lett. **78**, 967 (1997).

[8] J-E. Rubensson, S. Eisebitt, M. Nicodemus, T. Böske, and W. Eberhardt, Phys. Rev. B **49**, 1507 (1994); **50**, 9035 (1994).

[9] M. Elango, A. Ausmees, A. Kikas, E. Nommiste, R. Ruus, A. Saar, J. F. van Acker, J. N. Andersen, R. Nyholm, and I. Martinson, Phys. Rev. B **47**, 11 736 (1993).

[10] F. M. F. de Groot, Solid State Commun. **96**, 881 (1995).

[11] S. M. Butorin, J.-H. Guo, M. Magnuson, P. Kuiper, and J. Nordgren, Phys. Rev. B **54**, 4405 (1996).

[12] L. Braicovich, C. Dallera, G. Ghiringhelli, N. B. Brookes, J. B. Goedkoop, and M. A. van Veenendaal, Phys. Rev. B **55**, R15 989 (1997).

[13] N. F. Mott, Proc. Phys. Soc. London, Sect. A **62**, 416 (1949).

[14] For a review about NiO spectroscopy, see S. Hüfner, Adv. Phys. **43**, 183 (1994).

[15] G. A. Sawatzky and J. W. Allen, Phys. Rev. Lett. **53**, 2339 (1984).

[16] S. Hüfner and T. Riesterer, Phys. Rev. B **33**, 7267 (1986).

[17] M. Nakamura, Y. Takata, and N. Kosugi, J. Electron Spectrosc. Relat. Phenom. **78**, 115 (1996).

[18] O. Tjernberg, S. Söderholm, U. O. Karlsson, G. Chiaia, M. Quarford, H. Nylén, and I. Lindau, Phys. Rev. B **53**, 10 372 (1996).

[19] J. Goulon, N. B. Brookes, C. Gauthier, J. B. Goedkoop, C. Goulon-Ginet, M. Hagelstein, and A. Rogalev, Physica B **208&209**, 199 (1995).

[20] P. Elleaume, J. Synchrotron Radiat. **1**, 19 (1994).

[21] F. M. F. de Groot, J. Electron Spectrosc. Relat. Phenom. **67**, 529 (1994).

[22] A. Tanaka and T. Jo, J. Phys. Soc. Jpn. **63**, 2788 (1992).

[23] S. M. Butorin, D. C. Mancini, J. H. Guo, N. Wassdahl, J. Nordgren, M. Nakazawa, T. Uozumi, A. Kotani, Y. Ma, K. E. Myano, B. A. Karlin, and D. K. Shuh, Phys. Rev. Lett. **77**, 574 (1996).

[24] M. van Veenendaal and G. A. Sawatzky, Phys. Rev. Lett. **70**, 2459 (1993).

[25] In solid-state physics an example is given by the $2p3p3p$ and $2p3s3p$ Auger lines at the L_3 resonance in CuO. CuO is an insulator with a gap of $\sim$1.2 eV. The ground state is a mixture of the Cu $2p^6 3d^9$ and Cu $2p^6 3d^{10}\underline{L}$ configurations, so the intermediate state has pure Cu $2p^5 3d^{10}$ character. The core-hole potential pulls the intermediate-state binding energy well below the continuum. In this case, the Raman to Auger transition is observed only when the photon energy is high enough above threshold to excite electron-hole pairs across the gap. M. Finazzi, G. Ghiringhelli, O. Tjernberg, Ph. Ohresser, and N. B. Brookes (unpublished).

[26] M. F. López, A. Höhr, C. Laubschat, M. Domke, and G. Kaindl, Europhys. Lett. **20**, 357 (1992); Comment by L. H. Tjeng, *ibid.* **23**, 535 (1993); Reply by M. F. López, C. Laubschat, and G. Kaindl, *ibid.* **23**, 538 (1993); L. H. Tjeng, C. T. Chen, P. Rudolf, G. Meigs, G. van der Laan, and B. T. Thole, Phys. Rev. B **48**, 13 378 (1993); M. F. López, C. Laubschat, A. Gutierrez, A. Höhr, M. Domke, G. Kaindl, and M. Abbate, Z. Phys. B **95**, 9 (1994).

[27] F. M. F. de Groot, R. Ruus, and M. Elango, Phys. Rev. B **51**, 14 062 (1995).

[28] F. M. F. de Groot, Phys. Rev. B **53**, 7099 (1996).

[29] P. Carra, M. Fabrizio, and B. T. Thole, Phys. Rev. Lett. **74**, 3700 (1995).